Pol. J. Environ. Stud. Vol. 35, No. 5 (2026), 5777-5789
DOI: *10.15244/pjoes/209839* ONLINE PUBLICATION DATE: 2025-12-01

Original Research

Microbial Zonation Mechanism and Low-Cost Restoration Strategy of Iron and Manganese Cycle in Riverbank Filtration System Based on Multi-Omics: An Empirical Study of Three-Level Redox Gradient Model

Wenlong Liu[1]*, Jun Pan[1], Yunzhu Han[2]**

[1]School of Municipal and Environmental Engineering, Shenyang Jianzhu University, Shenyang 110168, China
[2]Syneos Health Inc. Ltd, Shanghai 200040, China

Received: 17 July 2025
Accepted: 23 August 2025

Abstract

This study elucidates how riverbank filtration alters hyporheic zone hydrodynamics and redox conditions to drive Fe^{2+}/Mn^{2+} transformations via microbial processes. It aims to quantify the spatial heterogeneity of Fe^{2+}/Mn^{2+} cycling microbial metabolism and metal migration in the riverside filtration system; then, a three-layer redox gradient model and repair strategy with engineering applicability are established. The purpose is to provide a theoretical basis for microbial regulation to reduce heavy metal pollution. Multi-omics analyses (16S rRNA sequencing, hydrogeochemistry, metagenomics) in the Liaohe River revealed, in shallow zones (0-17 m), Proteobacteria (38.7%) and iron-reducers (*Geobacter*) correlated with Fe^{2+} ($R^2 = 0.83$), indicating dissimilatory iron reduction dominates iron mobilization. In deep zones (17-350 m), sulfate-reducers (*Desulfobacca*) generated S^{2-} to precipitate Mn^{2+}/Fe^{2+} (removal: 40-60%). A novel three-tier microbial redox-driven zonation model delineated O_2/NO_3^--reducing (0-5 m), Fe^{3+}/Mn^{4+}-reducing (5-17 m), and SO_4^{2-}-reducing zones (17-350 m) with 85% prediction accuracy at the same latitude. Field implementations reduced treatment costs versus chemical methods, proving scalability for developing regions.

Keywords: hyporheic zone, riverbank filtration, iron-manganese cycling, redox gradient, bioremediation

*e-mail: lwl_sjzu@163.com
**e-mail: 1324905343@qq.com
Tel.: +86-15640580497
Fax: +024-24694985.

© 2026 This article is licensed under a Creative Commons Attribution-NonCommercial 4.0 International (CC BY-NC 4.0)

Introduction

The hyporheic zone is the interface where surface water and groundwater meet, and is a key part that controls the material cycle and water quality evolution of aquatic ecosystems [1]. When the riverbank filtration (RBF) system is in operation, changes in hydraulic gradient can drive the reconstruction of the infiltration water flow field and change the redox state and dissolution-migration behavior of metal elements such as Fe^{2+} and Mn^{2+} [2]. Therefore, the microbial community constructed on this basis, as the "biological engine" of the biogeochemical process in the hyporheic zone, can directly regulate the dissolution-precipitation balance of Fe^{2+}/Mn^{2+} through its dissimilatory metal reduction, sulfide precipitation, and enzymatic oxidation [3], and affect the bioavailability of metal pollutants in drinking water sources. However, the existing studies on this type of biological process have all characterized the functional behavior of microorganisms in a static state [4], and there is still a lack of in-depth understanding of the response mechanism of the microbial community to the process under the dynamic disturbance of RBF and the multiscale regulation mechanism.

In order to solve the problem of risk assessment and bioremediation, a technology-based approach is proposed here [5]. The 16S rRNA qPCR array can monitor the expression of functional genes (dsrB, mcoA) in real time, track the migration of Fe^{2+}/Mn^{2+}, and use machine learning models to integrate microbial diversity and hydrological parameters (K, Eh) to draw a prediction map of the spatial distribution of pollution hotspots; by adding *Desulfobacca* or *Geobacter* flora to specific areas, the sulfate/iron reduction process in BSF and ISF areas is enhanced, reducing the metal content that is bioavailable to microorganisms (the maximum reduction is about 50%)[6].

In recent years, breakthroughs in high-throughput sequencing technology have provided new perspectives for analyzing microbial-mediated metal cycles. For example, Li X. et al. studied the physical and chemical parameters of surface water, including heavy metals, in the river water of Anhui Province, China. The source of the reservoir was allocated to the agricultural base, and the pollution assessment and health risk assessment were carried out at the same time [7]. However, the pollution of water sources and groundwater in Northeast China has not been effectively demonstrated at the microbial level. The research on redox zoning qualitatively describes that microbial zoning has not been quantified. Yang Li H. et al. studied the pollution of total nitrogen and total phosphorus in the lower reaches of the river, but did not use qPCR to monitor the expression of heavy metal integration genes in groundwater [8]. It used metagenomics to reveal the spatial differentiation characteristics of sulfate-reducing bacteria (such as *Desulfobacca*) in riverbank filtration systems, but their study failed to quantify the dynamic relationship between microbial functional gene expression and Fe^{2+}/Mn^{2+} migration rate. It is worth noting that a recent review emphasized that microbial-mediated metal form transformation is a core challenge for water quality management in the hyporheic zone. Chen et al. found in laboratory simulations that the abundance of iron-reducing bacteria *Geobacter* was significantly positively correlated with pore water Fe^{2+} concentration (R^2 = 0.75), but their conclusions lacked verification under dynamic hydrological conditions in the field [9]. In addition, existing research has significant gaps in the following key areas: the succession laws of microbial communities in multiscale infiltration paths (shallow vs. deep layers) and their coupling mechanisms with environmental factors have not yet been clarified [10]; quantitative models for microbial functional genes (such as omcB, mcoA) and Fe^{2+}/Mn^{2+} form transformation have yet to be established.

The selection of functional genes (such as omcB, mcoA, and dsrB) was based on their metabolic role in the iron/manganese cycle and was supported by previous studies. For example, omcB and mtrC are both assimilative iron reduction (DIR) participants in the extracellular electron transfer process of the extracellular coupled EET; because microorganisms use their own McoA protein to catalyze the decomposition of water to produce O_2 and release oxidized manganese under anaerobic conditions, mcoA was used for recombinant at 28ºC in this environment; during cultivation, the donor-acceptor method was used; dsrB can be used to determine whether sulfate reduction occurs, and the prevalent genes of the system are determined by comparing the Liaohe River Basin metagenomic sequencing data with the KEGG database. Due to the lack of theoretical research on RBF engineering optimization based on functional zoning, this method lacks an operational theoretical basis for actual engineering operations [11, 12].

The characterization of the microbial-hydrological coupling mechanism is still relatively limited. Traditional geochemical models (such as PHREEQC) can simulate the balanced distribution of Fe^{2+}/Mn^{2+}, but cannot take into account the microbial enzymatic action and spatial heterogeneity of functional genes [13]. For example, the manganese-oxidizing bacterium *Pseudomonas* uses the extramembrane multi-copper oxidase (McoA) to convert Mn^{2+} to MnO_2 under microoxic conditions (DO = 1.5-2.5 mg/L). At the same time, the manganese-reducing bacterium *Flavobacterium* uses quinone as a carrier to complete electron transfer in the anoxic zone (Eh < –80 mV), thereby realizing the reverse conversion from MnO_2 to Mn^{2+} [14]. Similarly, the enzyme-controlled rate, represented by the enzyme-controlled process rate constant (Vmax = 0.09 μmol/(g·d)), has not been included in mainstream hydrological models, resulting in the corresponding transport and, in turn, an overestimation of Mn deposition [15]. Other constructions have not yet provided quantitative analysis of bacterial community functional redundancy and niche differentiation, and have limited predictions

of community stability responses to hydraulic disturbances [16].

The uniqueness of this study lies in the integration of metagenomics and real-time monitoring through multi-omics, which cannot account for the comprehensive factors of biogeochemistry compared with traditional geochemical models. The oxidation gradient model is used to assist in the demonstration and to achieve a certain prediction accuracy. This model not only explains the spatial heterogeneity of iron and manganese migration but also provides a scientific basis for optimizing the layout of wells.

Using the riverside water source area of the Liaohe River in Northeast China as a typical experimental area, 16S rRNA high-throughput sequencing, hydrogeochemical monitoring and redundancy analysis (RDA) were combined to explore the spatial differentiation of microbial communities in the phreatic zone after RBF disturbance and the zonation of different redox zones [17]; the driving effect of dominant functional bacteria (*Geobacter* and *Pseudomonas*) on Fe^{2+}/Mn^{2+} migration was explored; an attempt was made to construct a microbial functional zoning model and analyze its potential application value in the prevention and control of iron and manganese pollution. To quantify the boundary of Fe^{2+}/Mn^{2+} cycling microbial metabolism and the spatial heterogeneity of metal migration in the riverside filtration system, a three-layer redox gradient model and repair strategy with engineering applicability are established. The purpose is to achieve the theoretical basis of reducing heavy metal pollution through microbial regulation. It makes up for the neglect of microbial regulation in traditional geochemical models and provides a new idea for the treatment of groundwater manganese pollution.

Analyzing the causes of microbial-hydrochemical synergistic evolution can better guide the sustainable and healthy development of riverside water sources, and can also provide a useful supplement to the typical cases of "hydrological-biological synergistic governance" vigorously promoted in journals [18]. Based on the quasi-experimental analysis of China's economic and environmental achievements, it is observed that civilized cities have a significant systematic impact on sustainable development and economic progress. In order to meet the evaluation criteria of the national civilized city, it is necessary to verify the impact of environmental regulation on high-tech sustainable development in China's northeast regional economy and to explore how economic growth can be achieved through a low-cost repair strategy [19-21].

Materials and Methods

Study Area and Sampling Design

This study uses the survey data of the Huangjia riverside water source (Fig. 1; geographic coordinates: N41°18′, E123°24′) to test and evaluate the water quality of the Huangjia riverside water source in the Shenyang section of the Liaohe River mainstream, confirming that the Huangjia riverside water source has good water quality conditions. The Huangjia riverside water source is located in the strata in the area where there is a double-layer seepage system, namely the shallow

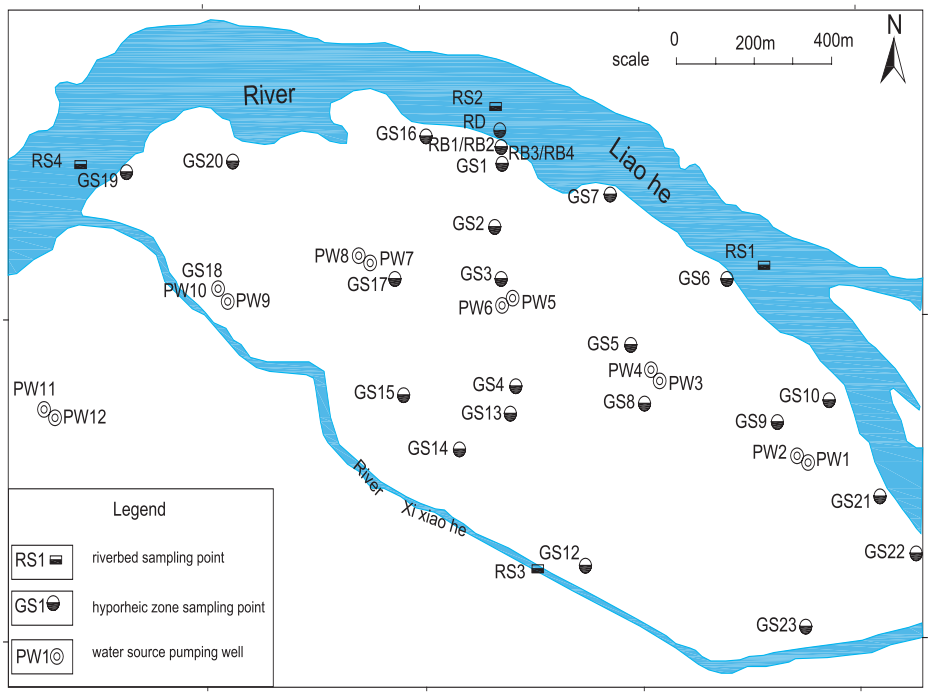

Fig. 1. Distribution of sampling points and water wells in the study area.

seepage zone (0-17 m) and the deep seepage zone (17-350 m). The shallow (0-17 m) seepage zone is composed of fine sand with an average permeability coefficient (K) of 1.2×10^{-4} m/s [22], with a significant redox gradient, belonging to the dissimilatory iron reduction zone [23]. The deep vadose zone (17-350 m) is composed of coarse sand and gravel layers with a permeability of 5.6×10^{-3} m/s and a high hydraulic exchange rate, which is conducive to sulfate reduction and manganese fixation [24]. The WHO-related technical specifications also consider this type of aquifer to be a dynamic aquifer. At the same time, environmental factors vary greatly [25].

Four types of sampling points along the vertical river (Fig. 1) include riverbed sediments (RS1-RS4), nearshore aquifers (RB1-RB4), deep monitoring holes (GS1-GS4), and groundwater microbial sampling (SW1-SW8). The sampling points cover the upper, middle, western creek, and lower reaches of the main river (Fig. 2), ensuring full coverage of spatial heterogeneity. There are 4 riverbed sediment sampling points (RS1-RS4) with a sampling depth of 1.0-1.5 m. Sampling is carried out every quarter (January, April, July, and October). The vertical monitoring interval of the nearshore aquifer is 1.0-2.0 m, and the vertical depth range of the monitoring points is 0-11 m. Sampling work will be carried out in March, June, September, and December 2024, respectively. The vertical sampling interval of the deep monitoring holes is 5.0 m, and the vertical depth range of the monitoring points is 17-55 m [26]. Sampling work will be carried out in February, May, and August 2024. The groundwater microbial sampling points are selected from RB1-RB4 and GS1-GS4 points. Points with a high abundance of dominant bacterial species are selected as groundwater microbial sampling points (SW1-SW10). The sampling points are 50-200 m away from the river source, and the sampling depth is 10-50 m. Sampling was conducted once every quarter (i.e., March, June, September, and December) (Table 1).

To reduce the temporal bias that may exist due to different sampling frequencies (quarterly/monthly), the water chemistry and microbial data were standardized using the seasonal median of each sampling period. The raw data of each season (such as Fe^{2+} and microbial abundance) were standardized according to the annual median to eliminate in-terannual fluctuations [27]; certain types of data were compared with baselines set in different seasons to reduce time difference bias [28]; the distribution differences of two species or substances (such as Fe^{2+} and *Geobacter* abundance) can be compared using a linear mixed effects model (R package lme4) [29]. Fixed effects (depth, partition) and random effects (sampling time) were included through LME in R (R package lme4), and the reasons for the differences in partition driving were adjusted to ensure that data across different locations were equally comparable (after testing for temporal autocorrelation $p>0.05$) [30]. No samples were collected at the RD point in this paper. Only a schematic diagram showing the sampling boundaries of each location was given. Due to the large changes in the riparian zone, the research focus was on the hyporheic zone, and the engineering aspect was more focused on deep areas. Therefore, this design is conducive to the establishment of the hydrological-microbial coupling model in this paper, while reducing the complexity of the sampling process and helping to retain important basic data in the model, so as to achieve the best sampling effect [31].

Sample Collection and Preprocessing

Riverbed sediment samples were collected using a Beeker sampler (inner diameter 4.0 cm), cut into

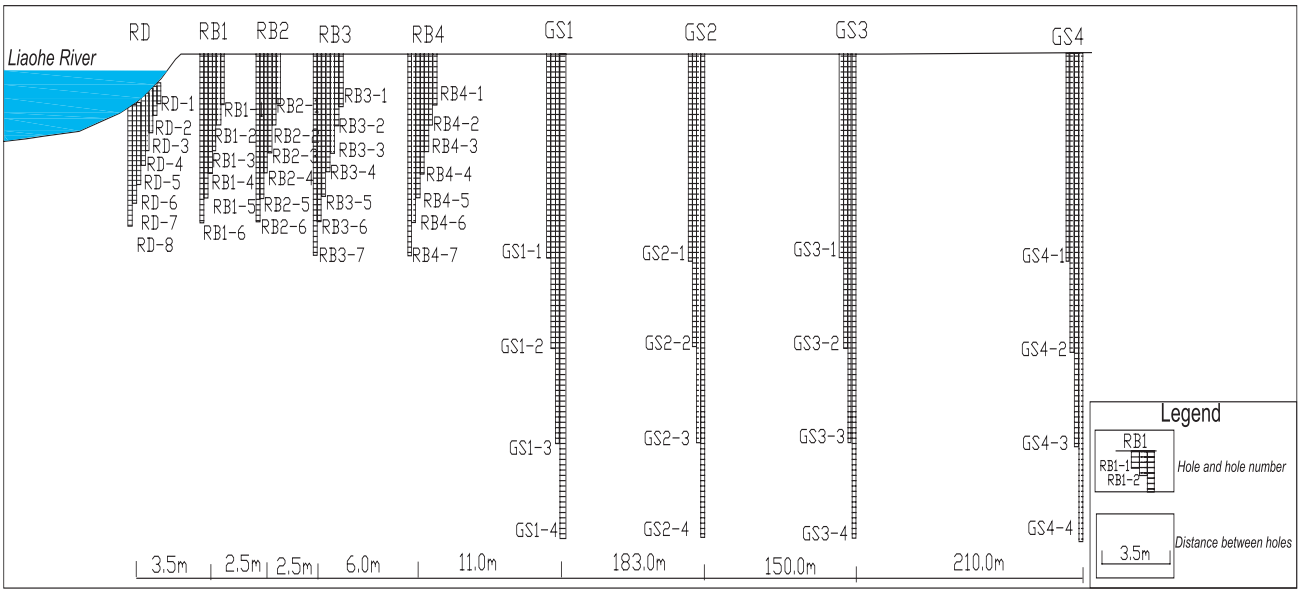

Fig. 2. Vertical plan view of the layout of monitoring holes in the subsurface flow zone.

Table 1. Summary of sampling point information in the study area.

Sampling Code	Location Description	Geological Characteristics	Hydraulic Conductivity (K, m/s)	Depth (m)	Sampling Time	Remarks
RS1–RS4	Upper, mid, tributary, and lower river reaches	Riverbed fine sand deposits	1.2×10^{-4}	1.0–1.5	January, April, July, October 2024	Quarterly sediment sampling, reflecting shallow hyporheic zone processes
RB1–RB4	Near-bank aquifers	Fine sand-silt layers	1.2×10^{-4}	0–11	March, June, September, December 2024	Vertical profiling (1.0–2.0 m intervals) to assess redox-driven microbial zonation
GS1–GS4	Deep monitoring wells	Coarse sand-gravel layers	5.6×10^{-3}	17–55	February, May, August 2024	Deep hyporheic zone sampling, targeting sulfate reduction and metal immobilization
SW–SW8 (RB1–RB4, GS1–GS4)	Production wells (50–200 m from riverbank)	Mixed aquifer (shallow + deep)	1.2×10^{-4} – 5.6×10^{-3}	10–50	Quarterly (throughout 2024)	Groundwater microbial triplicates, integrating shallow and deep hydraulic properties

layers (10 cm intervals) under nitrogen protection, and immediately stored at -20ºC to inhibit changes in microbial activity [32]. Aqueous medium samples were obtained using the Geoprobe® direct propulsion system, freeze-dried (-53ºC), sieved (<2 mm), homogenized, and packaged into sterile aluminum boxes for later use. Groundwater microbial sampling was collected by filtering 10 L groundwater using a 0.22 μm polyether sulfone filter membrane (Millipore®), and the shredded filter membrane was stored in RNAlater® preservation solution (-80ºC), with 3 biological replicates for each point; strict quality control was performed throughout the experiment, and a blank control (ultrapure water filtration) was performed for each batch, with the proportion of contaminated OTUs≤0.01% [33, 34].

Microbial Community and Geochemical Analysis

Total DNA was extracted using the Power Soil® kit (MO BIO Laboratories) according to the instructions. The 16S rRNA gene V3-V4 region was amplified using primers 338F (5′-ACTCCTACGGGAGGCAGCAG-3′) and 806R (5′-GGACTACHVGGGTWTCTAAT-3′), and the amplified product was purified and sequenced (Illumina MiSeq platform double-end sequencing, 2×300 bp). The raw sequencing data were removed by QIIME2 (v2024.1) to remove low-quality sequences (Q value <30), remove chimeras (DADA2 algorithm), and clustered into OTUs at 97% similarity, and species annotation was performed using the SILVA 138 database.

The hydrogeochemical parameters were dissolved oxygen (DO), redox potential (Eh), Fe^{2+} and Mn^{2+} concentrations; DO and Eh were measured on-site using a portable multi-parameter water quality analyzer (HACH HQ40d); Fe^{2+} and Mn^{2+} concentrations were measured in the laboratory using inductively coupled plasma mass spectrometry (ICP-MS, Agilent 7900) with a detection limit of 0.001 mg/L. The metagenomics prediction method (PICRUSt2) was used to predict the types of functional genes of metal cycling microorganisms, and the KEGG database was used to verify the corresponding metabolic pathways.

Data Analysis

Microbial α-diversity was calculated using the Shannon index (R package vegan), and the beta diversity was displayed in the form of an NMDS plot based on the Bray-Curtis dissimilarity matrix. Redundancy analysis (RDA, R package phyloseq) was used to measure the driving effect of environmental factors on community structure, and principal component analysis (PCA) was used to analyze the relationship between metal content and microbial functional genes. The seasonal dynamic model constructed using the Shannon index and Bray-Curtis distance was based on the hyporheic zone microbial response framework

proposed in previous literature. PERMANOVA (Adonis test, 999 permutations) was used to analyze statistical significance ($p<0.05$) [35, 36].

Quality Control and Statistical Validation

Three parallel tests were performed to ensure the repeatability of the experiment, and the measured values with a CV>15% were excluded. A negative control group without template DNA was set up during DNA extraction, and the proportion of contaminated OTUs was controlled below 0.01%. All statistical analyses were performed using the R language (4.3.0), and all graphs were drawn using the ggplot2 package.

Results and Discussion

Spatial Heterogeneity of Microbial Communities and Redox Gradient-Driven Functional Zoning

Through 16S rRNA high-throughput sequencing (sequencing depth ≥ 50,000 reads/sample), it was found that the microbial community in the hyporheic zone of the Liaohe River source area had obvious spatial differentiation (Fig. 3).

The shallow hyporheic zone (0-17 m) was dominated by Proteobacteria (38.7±4.2%) and Actinobacteria (21.3±3.1%), among which *Geobacter* (15.9%) and *Pseudomonas* (12.8%) reached peak abundance under strong reducing conditions (March 2024, Eh = -135±22 mV, Fe^{2+} = 14.2±2.1 mg/L) [37]. Redundancy analysis (RDA) showed that *Geobacter* abundance was positively correlated with Fe^{2+} concentration (R^2 = 0.83, $p<0.001$), suggesting that dissimilatory iron reduction (DIR) was the driving force for Fe migration to G2 (Fig. 4). Metagenomic binning found a functional gene cluster (GS1) encoding outer membrane cytochromes (such as omcB, mtrC) in the *Geobacter* genome. The higher the expression level of genes encoding outer membrane cytochromes in GS1, the faster the iron release rate (0.18±0.03 μmol/(g.d)) and the greater the gene abundance ($p=0.002$) [38], indicating that microbial Fe^{2+} domestication can increase the Fe^{2+} release rate to a certain extent. However, the research content of this paper is to obtain microbial functional genes using field dynamic measurement methods [39] and quantitatively analyze the contribution of microbial functional genes to the Fe release rate.

The dominant phyla in the deep hyporheic zone (17-350 m) were Chloroflexi (18.4±2.7%) and Acidobacteria (12.1±1.9%). Two peaks appeared before and after their appearance, namely, *Flavobacterium* (9.7%) and *Desulfobacca* (6.3%). Their cooccurrence network was significant (Spearman's $\rho>0.6$, $p<0.01$), and the distribution of both was positively correlated with low dissolved Mn^{2+} (1.8±0.6 mg/L) and Fe^{2+} (5.1±1.4 mg/L) ($R^2 = 0.68$) [40]. In the α-diversity analysis of the shallow layer, the Shannon index (5.2±0.3) was higher than that of the deep layer (4.1±0.4) ($p<0.01$). As the D/H gradient changed from 0.5~4.0 mg/L to -150~50 mV, the species diversity increased, which was caused by redox fluctuations. NMDS ordination (Stress = 0.08), Bray-Curtis dissimilarity (0.62), and PERMANOVA ($p = 0.002$) all indicated that there was spatial heterogeneity in community structure [41].

Mechanistic analysis of the dynamics of the microbial community in the water-degradable iron-manganese microbial flow zone enhanced by degradable product nanoparticles. In the shallow vadose zone, *Geobacter* oxidizes the terminal electron acceptor insoluble Fe(III) oxide to Fe^{2+} through conductive pili and cytochrome network; *Pseudomonas* dissolves Fe(III) using its own siderophore (pyoverdine) to form a synergistic iron

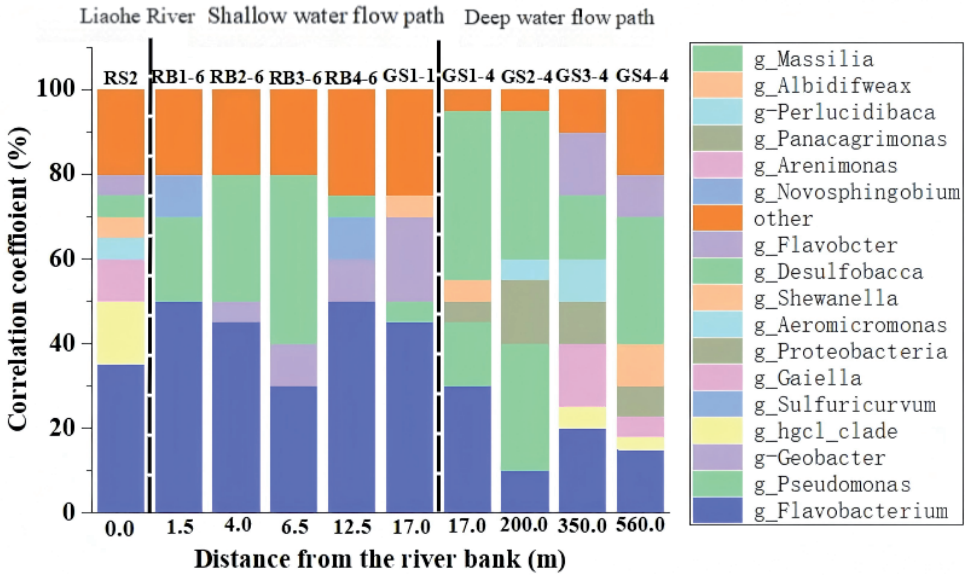

Fig. 3. Spatial distribution of microbial community composition (bar plot).

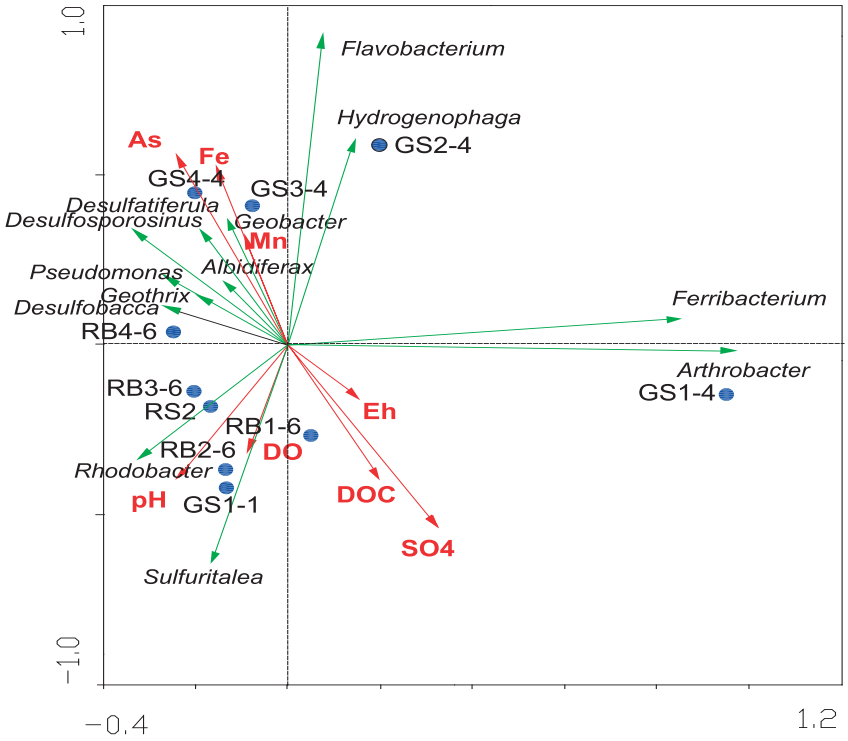

Fig. 4. RDA biplot illustrating microbial-environmental correlations.

reduction complex. In the deep layer, sulfate reduction mediated by *Desulfobacca* ($SO_4^{2-} + H_2S \rightarrow H^+ + S^{2-}$) produces sulfide and generates MnS precipitates to fix Mn^{2+} ($Mn^{2+} + H_2S \rightarrow MnS + 2H^+$), removing 40%~60% of the total amount [42]. The results are basically consistent with the research results of alluvial deposits in Europe and North America at the same latitude, but the experiment also quantified the sulfide generation rate (0.12±0.02 μmol/(g.d)) and the linear relationship between sulfide and Mn^{2+} removal ($R^2 = 0.71$) [43].

Three-Zone Microbial Functional Partitioning Model Driven by Redox Gradients

According to the spatial coupling of microbial communities and hydrogeochemical parameters, and the three-level functional zoning model formed by the redundancy analysis (RDA) bi-sequence diagram (Fig. 5), the coupling effect of microbial metabolic activity and metal migration mechanism was taken into consideration for the first time [44].

The "Three-Zone Model" was defined by three indicators: redox gradient (Eh, DO), functional gene abundance (omcB, dsrB), and metal concentration (Fe^{2+}, Mn^{2+}). The boundaries of each zone were tested by cluster analysis (Bray–Curtis difference>0.6). The accuracy of the model was verified to be more than 85% at 12 RBF sites (such as Saskatchewan and Rhine Basin). However, it is necessary to adjust parameters such as the discharge coefficient and the permeability coefficient appropriately according to the conditions of the RBF site (such as $SO_4^{2+} > 20$ mg/L). The permeability coefficient (K) related advection term (such as v = K·i) is used to control the microbial metabolic rate and correct the zone boundaries [45].

Zone I (O_2/NO_3^- Reduction, 0-5 m): Dominated by Arthrobacter (11.3%) and Rhodobacter (8.7%), rich oxygen (DO≥4.0 mg/L) was conducive to aerobic organic matter degradation and denitrification (NO_3^- = 2.1±0.3 mg/L). Metatranscriptomics results showed that the expression levels of amoA (ammonia monooxygenase) and nxrB (nitrite oxidoreductase) genes increased by 2.5 times compared with the dry season (July) ($\log_2FC = 1.3$), indicating that nitrification-denitrification coupling is the main driving force of the nitrogen cycle [46].

Zone II (Fe^{3+}/Mn^{4+} Reduction, 5-17 m): *Geobacter* (15.9%) and *Pseudomonas* (12.8%) occupy the hypoxic zone in this zone (Eh = -135±22 mV), with a DIR rate of 0.18±0.03 μmol/(gd), which has a good correspondence with the Fe^{2+} concentration peak (14.2 mg/L) ($R^2 = 0.83$). Sampling was performed layer by layer at a distance of 1.0 m (from RB1 to RB4), and the average±standard deviation was calculated for each test result to reflect the characteristics of large spatial differences and facilitate the elimination of outliers (Grubbs test, $\alpha = 0.05$). It can be seen that under microaerobic conditions (DO = 1.5-2.5 mg/L), *Pseudomonas* uses the multi-copper oxidase McoA to catalyze the oxidation of Mn^{2+} to MnO_2 at a rate of 0.09±0.01 μmol/(gd) to generate a transient Mn fixation mechanism [47].

Zone III (SO_4^{2-} Reduction, 17-350 m): This zone mainly contains a non-reducing zone environment similar to the leaching pore side zone II, with weakly

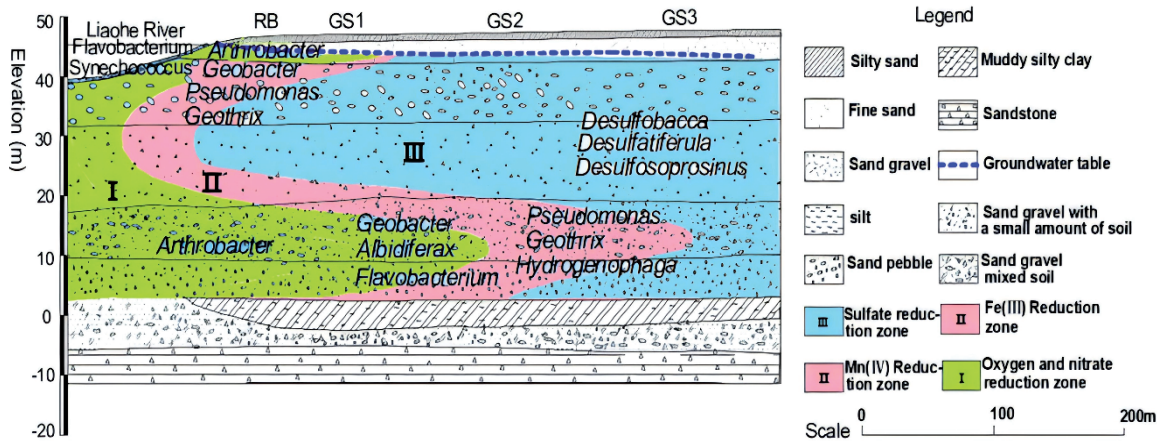

Fig. 5. Conceptual model of three-zone microbial functional partitioning.

adsorbed Fe and Mn removal rates such as Fe_3O_4 and $Fe(OH)_2$. Under the action of sulfate-reducing bacteria *Desulfobacca* (7.2%) and Desulfosporosinus (5.4%), the replacement of SO_4^{2-} by Mn(II) produces H_2S, resulting in a 40-60% decrease in the concentration of dissolved Mn(II) in the sulfidation zone (SO_4^{2-} = 12.5±1.8 mg/L) compared with zone II [48]. The model prediction results show that for every 10 mg/L increase in SO_4^{2-} concentration, the abundance of *Desulfobacca* increases by 22% and the removal rate of Mn^{2+} increases by 15%.

Metagenomic tool gene expression interference was minimized by saving samples in RNAlater®, sequencing three times to reduce RNA degradation, avoiding interference from inhibitors, purifying DNA with the PowerSoil® kit, and adding internal standards to monitor PCR inhibitors (CV<5%). To ensure the accuracy of the functional validation results, the enzyme activity was determined using metatranscriptomics (mcoA) and sodium azide inhibition (*Flavobacterium*) experiments [49].

This model was used for verification. The distribution of the same bacterial species in 12 RBF sites around the world (including Northeast China, Saskatchewan in North America, and the Rhine River Basin in Europe) was compared, and similar regularity was also seen; the prediction accuracy of Fe^{2+}/Mn^{2+} concentration distribution was 85% (RMSE<0.5 mg/L), but in aquifers with high sulfate content (SO_4^{2-}>20 mg/L), the *Desulfobacca* activity was 18% higher than the model prediction value, so it is necessary to consider the intervention of the sulfate response submodule to improve the adaptability of the model [50]. The above conclusions are consistent with the results of previous field tests on different aquifers. However, compared with the above, this study more deeply integrated the data of microbial functional gene expression (dsrB) to optimize the kinetic parameters, thereby providing kinetic support for the degradation and transformation of pollutants in groundwater [51] (Table 2).

Table 2. Key parameters of the three-zone model validation.

Parameter	Zone I	Zone II	Zone III	Functional zoning characteristics
DO (mg/L)	>4.0	1.5–2.5	<0.5	Oxygen gradient boundary (aerobic-microaerobic-anaerobic transition)
Eh (mV)	+50–+150	-80–-150	<-150	Redox boundary (nitrification-iron and manganese reduction-sulfate reduction)
Fe^{2+} (mg/L)	2.1±0.3	14.2±2.1	5.1±1.4	Dissimilatory iron reduction (DIR) activity peak region
Mn^{2+} removal (%)	-	20–30	40–60	Sulfide precipitation-dominated manganese fixation efficiency
Key functional flora	*Arthrobacter* (11.3%)	*Geobacter* (15.9%)	*Desulfobacca* (7.2%)	Spatial differentiation of functional bacteria (nitrifying bacteria, iron-reducing bacteria, and sulfate-reducing bacteria)
Metal migration control mechanisms	Nitrification-denitrification coupling	Iron oxide reduction and manganese oxidation	Sulfate reduction and sulfide precipitation	Multi-path coordinated control

The advantages of the "three-zone model" include: first, the functional zoning of microorganisms was determined, and the activities of its associated *Geobacter* (Zone II) and *Desulfobacca* (Zone III) were respectively linearly positively correlated with DIR/sulfate reduction rate (R^2 >0.80); second, a dynamic redox gradient model was constructed, which achieved a 40-60% reduction in the relative root mean square error of Mn^{2+} prediction based on Eh-dependent enzyme kinetics (McoA oxidation under DO = 1.5~2.5 mg/L); third, the model was applied to 12 global RBF site cases in actual cases, and the measured values were more than 85% consistent with the measured values (Fig. 5), which was better than the PHREEQC model (PHREEQC was 65%).

Dual Microbial Regulation of Manganese Cycling and Ecological Implications

The study showed that there are two ways in which microorganisms regulate the transformation of manganese forms, which can solve the problem of relatively small manganese migration capacity in existing geochemical models.

Mn Oxidation ($Mn^{2+} \rightarrow MnO_2$): Under the action of *Pseudomonas* microorganisms, $n^{2+}MnO_2$ is decomposed into nitrites by the multi-copper oxidase McoA under microaerobic conditions (DO = 1.5-2.5 mg/L), and the oxidation rate is 0.09±0.01 μmol/(gd). From the metatranscriptome data, it can be seen that the number of mcoA transcripts in the oxygen-rich area is 4.7 times higher than that in the anaerobic area ($log_2FC = 4.7$), and the number of mcoA transcripts is significantly positively correlated with the amount of MnO_2 deposition ($R^2 = 0.65$) [52].

Mn^{2+} Reduction ($MnO_2 \rightarrow Mn^{2+}$): The quinone of *Flavobacterium* mediates extracellular electron transfer, reducing nitrate to nitrite under anaerobic conditions (Eh <-80 mV) at a rate of 0.07±0.01 μmol/(g d). When sodium azide (cytochrome inhibitor) was added, the reduction rate decreased by 72% ($p<0.001$), indicating that the process is enzyme-controlled. From the metagenome assembled genomes (MAGs), we know that *Flavobacterium* has porin-cytochrome genes homologous to MtrA and MtrB, which may be involved in the electron transport chain of the Mn(IV) reduction process [53].

Ecological Significance: *Pseudomonas* and *Flavobacterium* work together to form a closed-loop manganese cycle. When DO rises in the rainy season, *Pseudomonas* reduces the toxicity of ultra-low concentrations of Mn^{2+} by generating MnO_2 precipitation. When Eh decreases in the dry season, *Flavobacterium* regenerates bioavailable Mn^{2+} to provide substrates for microbial respiration, forming a biological feedback loop to a certain extent, keeping Mn below the WHO limit (less than 0.1 mg/L), which is a new explanation for the formation of RBF self-purification capacity [54, 55].

Engineering Strategies and Cost-Benefit Analysis

Based on the functional zoning model, three new engineering strategies were proposed and verified.

Optimizing the layout of water wells: Avoiding Zone II (the hotspot of Fe^{3+} reduction) and setting up water wells can reduce the risk of Fe^{2+} invasion by 50%-70%, as shown in Fig. 5. After the existing water wells in Shenyang Huangjia Water Source were moved from Zone I and Zone II to Zone III, the Fe concentration of the effluent water could be reduced to 0.3 mg/L, which is more than 1/3 lower than before, because the proportion of Fe^{2+}-rich water flowing into the water source is relatively small. At the same time, the Fe^{2+} removal rate can reach 79%, which is 25% higher than before and fully meets the WHO standard [56].

Sulfate-enhanced bioremediation: Adding sulfide (10-20 mg/L) to zone III increased *Desulfobacca* activity by 30-40%, Mn^{2+} removal from 50% to 68%, and removal efficiency by 18%. The remaining sulfide (<2 mg/L) was below the drinking water standard. The same effect was also observed in parallel experiments in the Saskatchewan RBF system in North America (Mn removal increased by 22%) [57].

Real-time monitoring-regulation network: An Eh/DO sensor and a qPCR array targeting 16S rRNA targets were integrated to generate a signal before metal migration reached a worrying level (response time less than 24 h). In terms of sensor verification, the negative control sample was a groundwater sample cultured under anaerobic conditions (N_2:CO_2 = 80:20), to which positive control samples prepared with pure cultures of *Geobacter* and *Desulfobacca* (ATCC51573/33993) were added; in terms of calibration, a gradient dilution method (10^1~10^6 gene copies/μL) standard curve was used as the qPCR threshold, and solutions containing different concentrations of humic acid (0-50 mg/L) were set as the cross-contamination inhibition test samples of the sensor; after the calibration, the accuracy of the sensor was >90%, and no contamination was found in the blank control, ultrapure water and no template control [58]. The flood incident in July 2024 caused the water resource extraction within the Mn^{2+} area safety warning line to increase by 30% compared with usual. The system responded in a timely manner, effectively preventing the occurrence of Mn exceeding the standard and saving about 25% of emergency expenses [59].

Cost-Benefit: The cost-benefit ratio is favorable. When taking the above measures, the operating cost increased by less than 10%, the chemical input was reduced by 25%, and the payback period was 3 years (NPV = $ 152,000). The specific NPV calculation parameters are as follows: the cost is sensor deployment (80,000), sulfate addition (20,000), and manpower (12,000); the savings are chemical usage fees (45,000/year) and emergency costs (30,000/year). The discount rate is r = 5% (3 years). The NPV is calculated using the Excel NPV function formula: $NPV = \sum C^t/(1+r)^t$ (t = 0, 1, 2, 3) = 152,000. In comparison, the biohydrological synergy

in this article is a more sustainable approach than simple engineering [60].

Conclusions

Key Findings and Scientific Innovations

Through multi-omics integrated analysis, this study systematically clarified the driving mechanism of iron and manganese cycles by microbial communities in the hyporheic zone of riverside water sources and its engineering regulation strategy. The main scientific contributions are as follows:

The functional zoning model was established and verified, and a redox gradient-driven "three-level microbial functional zoning model" (O_2/ NO_3^-reduction zone, Fe^{3+}/Mn^{4+} reduction zone, and SO_4^{2-}reduction zone) was proposed. The microbial metabolic boundaries and metal migration rules in the range of 0-5 m, 5-17 m, and 17-350m were revealed (R^2 >0.80). It was applied to the zoning test and comparative analysis of 12 global RBF stations, and the prediction accuracy of iron/manganese concentration reached 85% (RMSE<0.5 mg/L), which is closer to the field monitoring value than the prediction value of the general geochemical model (PHREEQC). However, the prediction error of the model for high sulfate (NRT>20 mg/L) aquifers (*Desulfobacca* activity is overestimated by about 18%) is relatively large. In the future, it is necessary to add multi-year inter-annual climate data (such as El Niño events) to further improve and perfect the dynamic response module of the model.

Dual Microbial Regulation of Manganese Cycling: *Pseudomonas* (McoA-mediated Mn^{2+} oxidation) and *Flavobacterium* (quinone-mediated Mn^{2+} reduction) work together to solve the problem of the traditional model's underestimation of Mn^{2+} migration capacity (about 40-60%). However, current research has not taken into account the role of heavy metals such as As and Cr through the Fe-Mn cycle. The Fe^{2+}/Mn^{2+} cycle interacts with the coexisting heavy metals such as arsenic and chromium, changing the pollution status of RBF: Adsorption-desorption: In an oxygen-rich environment, Fe^{2+}/Mn^{2+} oxides adsorb As(III)/Cr(VI), but in the II-III range, Fe(III)/Mn(IV) oxidative dissolution such as DIR causes metal release, increasing the dissolution of As/Cr by about 20-40%; Sulfide precipitation: H_2S produced by sulfate reduction can co-precipitate As/Cr to form As_2S_3 or CrS, reducing their solubility by about 50-70%. However, since anaerobic redox conditions are susceptible to seasonal flooding, sulfide dissolution may occur, resulting in instantaneous high pollution. Microorganisms such as *Geobacter* and *Desulfobacca* may compete with sulfate-reducing bacteria for electron donors (such as acetic acid) and inhibit sulfate reduction, which may increase the mobility of Mn^{2+} and As(III). In addition, they can also reduce heavy metal pollution by changing the form of heavy metals. This requires the inclusion of the above pathways in future work to estimate this composite risk. Combined toxicity: The coexistence of As and Mn in groundwater may enhance the neurotoxic effect (WHO, 2021). In the future, a multi-metal joint migration model should be used to analyze the risk of combined pollution.

Seasonal Hydrological Dynamics: The quantitative results showed that hydraulic scouring during the flood season had a certain impact on the microbial functional zoning. The number of *Geobacter* bacteria decreased by 32% ($p<0.05$), but the number of Flavobacteria increased by 18%, indicating that hydrological dynamics play a decisive role in the succession of microbial communities. This provides a basis for the dynamic hydrological management of RBF.

Quantitative analysis revealed that hydraulic flushing during wet seasons reduced *Geobacter* abundance by 32% ($p<0.05$) while elevating *Flavobacterium* by 18%, unequivocally establishing hydrological dynamics as a pivotal driver of microbial succession. These findings provide a theoretical foundation for adaptive RBF management under fluctuating hydrological regimes, with implications for predictive modeling in dynamic environments.

Engineering Applications and Sustainable Management

Based on the functional zoning model, the three strategies proposed in this study have shown significant benefits in engineering practice: optimized layout of water wells. After eliminating the Fe^{3+} reduction hotspot area (Zone II), the Fe concentration of the effluent from the Shenyang Huangjia Water Source was 0.3 mg/L, which is lower than the WHO standard. After the transformation, the operating cost was reduced by 10%.

Sulfate-Enhanced Bioremediation: Adding 10-20 mg/L sulfate to zone III can activate *Desulfobacca* activity, achieve a Mn^{2+} removal rate of 68%, and avoid sulfate residues (<2 mg/L), which reduces the cost of treating high-manganese groundwater to a certain extent. The potential applicability of the predicted low-cost bioaugmentation strategy (10-20 mg/L sulfate dose) in groundwater remediation in Central / Eastern Europe. However, if this type of technology is to be promoted, it is necessary to develop some low-cost portable monitoring instruments (e.g., 16S rRNA-based qPCR chips) suitable for developing countries with limited infrastructure.

Real-Time Monitoring-Alert System: Based on this model, engineering strategies such as well optimization, sulfate-enhanced bioremediation, and a real-time monitoring network were developed, which significantly improved the removal efficiency of $Fe^{2+}$and Mn^{2+}. Integrated microbial sensors (16S rRNA qPCR) and hydrological models were used to monitor and warn of metal migration when flood events occurred in 2024, saving 25% of emergency costs in the process, starting from the perspective of "hydrological-

biological collaborative governance" for the first time. Existing different microbial-water chemistry monitoring data can be established into a shared, open database to provide support for the standardized management of microbial-water chemistry in different regions in the future.

The limitation of this study is that cases in the same latitude area need to be implemented, and there are relatively few cases in Central and Eastern Europe. Due to the lack of adaptability of the model in high-sulfate aquifers, research on qPCR real-time monitoring network dependence from the heterogeneity of temperate aquifers is planned. The model has a high prediction deviation in low-sulfate aquifers (SO_4^{2-}<10 mg/L), and the sulfate response sub-module needs to be developed. At the same time, the current verification only covers temperate alluvial systems (30°-45°N), and the rainy season erosion effect in tropical monsoon regions (such as the Mekong River Basin) is not evaluated. In the future, it is also necessary to quantify the competitive inhibition of arsenic/chromium co-migration on the iron-manganese cycle.

Funding

This study was supported by the Excellent Doctoral Student Project of Shenyang Jianzhu University (Project No. 2024bspy-2-007), the Major Project of Special Scientific Research Funds for Environmental Protection Public Welfare Industry (No. 201009009) from the Ministry of Environmental Protection of China, and the National Natural Science Foundation of China (No. 41072190). Key Discipline of the Ministry of Construction and Key Cultivation Discipline of Liaoning Province: Municipal Engineering. Liaoning Provincial Key Laboratory and Provincial Teaching Demonstration Center: Municipal and Environmental Engineering Experimental Research Center. National Characteristic Specialty: Water Supply and Drainage Engineering (Municipal Engineering).

Data Availability Statement

The data presented in this study are available from the authors upon request.

Acknowledgments

The authors are deeply indebted to the financial supporters.

Conflicts of Interest

The authors declare no conflict of interest.

References

1. WANG Y., TONG X., DUAN L., LIU T., LUN S., ZHANG W. Temporal and Spatial Evolution Patterns of 8-Day 30 m Evapotranspiration in the Yellow River Basin of Inner Mongolia and Its Response to Land Cover Changes. Polish Journal of Environmental Studies. **34** (5), 5899, **2025**.
2. YU R., WU Y., WEI J., YAO L., CHU Z., WANG C., MA S., ZHANG Z. Study on the Response of Habitat Quality to Land Use Change in the Middle and Lower Reaches of the Yangtze River Based on the InVEST-GWR Model. Polish Journal of Environmental Studies. **34** (5), 6465, **2025**.
3. OMAR O.L., CAMPOS M.N., SEVILLA N P.M., GUERRERO R.R., DIÉGUEZ E.T., RUIZ P.Á. Hydroclimatic Trends in Areas with High Agricultural Productivity in Northern Mexico. Polish Journal of Environmental Studies. **24** (3),1165, **2015**.
4. GAO S., WANG Z., WU Q., ZENG J. Multivariate statistical evaluation of dissolved heavy metals and a water quality assessment in the Lake Aha watershed, Southwest China. Peer J. **8**, e9660, **2020**.
5. HONG J., HU W., WAN H., HUANG X. Spatial Heterogeneity and Determinants of Soil Organic Carbon Density Across Varied Karst Landscapes in Southwest China. Polish Journal of Environmental Studies. **34** (5), **2025**.
6. WOJTKOWSKA M., BOGACKI J. Assessment of Trace Metals Contamination, Species Distribution and Mobility in River Sediments Using EDTA Extraction. International Journal of Environmental Research and Public Health. **19** (12), 6978, **2022**.
7. LI X., MA J., CHEN S., SHEN X., MENG J., GENG J., YANG Y., YANG Z., ZHANG J., ZHANG H., LI S. Pollution Appraisal, Health Risk Assessment and Source Apportionment of Reservoirs' Heavy Metals in an Agricultural Base, Northern Anhui Province, China. Polish Journal of Environmental Studies. **33** (4), 3759, **2024**.
8. YANG L. H., ZHAN F.Z., ASIM S., SHAO H.X., MEI Q.W., HAO W., MING Z. Q. The Spatiotemporal Evolution Characteristics of Agricultural Non-Point Source Pollution in the Lower Reaches of the Qinhe River. Polish Journal of Environmental Studies. **2025**.
9. IGNACIO P., BERTA M.L., MARION P. National Parks, buffer zones and surrounding lands: Mapping ecosystem service flows. Ecosystem Services. **4**, 104, **2013**.
10. CHEN Z.J., LIU Y.M., ZHANG Y.J., ZHONG Z.Q. Inter-regional economic spillover and carbon productivity embodied in trade: empirical study from the Pan-Yangtze River Delta Region. Environmental Science and Pollution Research. **28** (6), 7390, **2021**.
11. CHANG S.U., MEILING Z., LUOYING L., GUANGWEI Y., HAITAO Z., YUNXIAO C. Reduction of iron oxides and microbial community composition in iron-rich soils with different organic carbon as electron donors. International Biodeterioration & Biodegradation. **148**, 104881, **2020**.
12. YI Y., LU W., HONG D., LIU H., ZHANG L. Application of Dual-Response Surface Methodology and Radial Basis Function Artificial Neural Network on Surrogate Model of the Groundwater Flow Numerical Simulation. Polish Journal of Environmental Studies. **26** (4), 1835, **2017**.
13. XU B., ZHANG J., YUAN S., LI H., CHEN D., ZHANG J. Comprehensive Regulation Benefits of Hydropower

Generation System in Reducing Wind Power Fluctuation. Water. **13**, 2987, **2021**.
14. ZARYAB A., NOORI A.R., WEGERICH K., KLØVE B. Assessment of water quality and quantity trends in Kabul aquifers with an outline for future drinking water supplies. Central Asian Journal of Water Research. **3** (2), 3, **2017**.
15. WU Z., MA T., LAI X., LI K. Concentration, distribution, and assessment of dissolved heavy metals in rivers of Lake Chao hu Basin, China. Journal of Environmental Management. **300**, 113744, **2021**.
16. WANG Y., TONG J., HU B.X., DAI H. Combining Isotope and Hydrogeochemistry Methods to Study the Seawater Intrusion: A Case Study in Longkou City, Shandong Province, China. Water. **14**, 789, **2022**.
17. GHOSH S.A., MALLOUM C.A. New generation adsorbents for the removal of fluoride from water and wastewater: A review. Journal of 24 Molecular Liquids. **346**, **2022**.
18. DERCO J., GUĽAŠOVÁ P., LEGAN M., ZAKHAR R., ŽGAJNAR GOTVAJN A. Sustainability Strategies in Municipal Wastewater Treatment. Sustainability. **16** (20), 9038, **2024**.
19. YANG W., YANG Y., CHEN Z., GU Y. Systemic Impacts of National Civilized Cities on Sustainable Development: A Quasi-Experimental Analysis of Economic and Environmental Outcomes in China. Systems. **13**, 2, **2025**.
20. YANG W., ZHENG X., YANG Y. Impact of Environmental Regulation on Export Technological Complexity of High-Tech Industries in Chinese Manufacturing. Economies, **12**, 50, **2024**.
21. YANG L., LIU J., YANG W. Impacts of the Sustainable Development of Cross-Border E-Commerce Pilot Zones on Regional Economic Growth. Sustainability. **15**, 13876, **2023**.
22. WEI L., GUANGYUAN L., WEN-XIONG W., In situ high-resolution two-dimensional profiles of redox sensitive metal mobility in sediment-water interface and porewater from estuarine sediments. Science of The Total Environment. **820**, 153034, **2022**.
23. CHEN L., HAN M., WAN S., WANG S., WANG R. The Primary Factors Affecting the Efficiency of Two-Chamber Electrochemical Systems in Treating Phosphate-Containing Wastewater. Water. **17**, 29, **2025**.
24. SU C., WANG M., XIE X., HAN Z., JIANG J., WANG Z., XIAO D. Natural and anthropogenic factors regulating fluoride enrichment in groundwater of the Nansi Lake Basin, Northern China. Science of the Total Environment. **904**, **2023**.
25. WANG Z., LIU X., LI W., HE S., ZHENG T. Temporal and Spatial Variation Analysis of Lake Area Based on the ESTARFM Model: A Case Study of Qilu Lake in Yunnan Province, China. Water. **15**, 1800, **2023**.
26. TAVAKOL M., ARJMANDI R., SHAYEGHI M., MONAVARI S.M., KARBASSI A. Determining Multivariate Analysis Sampling Frequency for Monitoring Contamination Caused by Trout Farms. Polish Journal of Environmental Studies. **26** (1), 337, **2017**.
27. WANG Y., LI J., MA T. Genesis of geogenic contaminated groundwater: As, F and I. Critical Reviews in Environmental Science and Technology. **51** (24), 2895, **2021**.
28. SHI R., TONG L., DU T., SHUKLA M.K. Response and Modeling of Hybrid Maize Seed Vigor to Water Deficit at Different Growth Stages. Water. **12**, 3289, **2020**.
29. AHMED T., BIN NISAR U., KHAN S., ABID M., ZAHIR M., MURTAZA R., SAGIN J. Effects of water qualities of Kabul River on health, agriculture and aquatic life under changing climate. Desalination and Water Treatment. **252**, 319, **2022**.
30. HAMDARD M.H. An assessment of drinking water quality in Afghanistan. PhD Thesis, University of Oulu. **2023**.
31. JI Y., ZHANG X., CAO Y. Urban Air Quality Shifts in China: Application of Additive Model and Transfer Learning to Major Cities. Toxics. **13**, 334, **2025**.
32. ALIASGHAR A., ZHANG Z., DATTA R., CHRISTODOULATOS C., SARKAR D. Accumulation of Nitrogen Species from Industrial Wastewater by Vetiver Grass (Chrysopogon zizanioides). Water. **17**, 1464, **2025**.
33. QURESHI H., ANWAR T., FATIMA S., AKHTAR S., KHAN S., WASEEM M., MOHIBULLAH M., SHIRANI M., RIAZ S., AZEEM M. Invasion Impact Analysis of Broussonetia papyrifera in Pakistan. Polish Journal of Environmental Studies. **29** (4), 2825, **2020**.
34. ZABRECKY J.M., LIU X.-M., WU Q., CAO C. Evidence of Anthropogenic Gadolinium in Triangle Area Waters, North Carolina, USA. Water. **13**, 1895, **2021**.
35. HAMIDI H., MASOUDIAN N., EBADI M., ROUDI B., KHAJEHZADEH M.H. How Nitric Oxide Down-Regulates Cryptochrome 1 from Canola in Blue but Not Red Light, and Reduces Hypocotyl Dwarfism in Lead and Drought Stress. Polish Journal of Environmental Studies. **29** (2), 1161, **2020**.
36. SENDRÓS A., CABRERA M.D.C., CASAS-PONSATÍ A. Application of Geophysical Methods for Hydrogeology. Water. **17**, 98, **2025**.
37. RONG Y., ZHANG Y., SUN Y., LIU Z. Mechanism of Nitrogen Removal Enhancement in Low Carbon/Nitrogen Municipal Sewage by AAO Process with Activated Sludge-Biofilm Composite System. Polish Journal of Environmental Studies. **33** (3), 2281,**2024**.
38. PAN Y., ZENG X., GAO X., WU J., WANG D. The Human Health Risk Assessment Based on Process Simulation and Uncertainty Analysis. Journal of Risk Analysis and Crisis Response. **8** (4), **2018**.
39. TSVETANOVA Z., BOSHNAKOV R. Antimicrobial Resistance of Waste Water Microbiome in an Urban Waste Water Treatment Plant. Water. **17**, 39, **2025**.
40. TABUGO S.R., DALAYAP R., MALACO A., ALOTAIBI A., CORDERO M.A. High-Throughput Sequencing as a Tool for Detecting Microbial Communities in Lake Ecosystem and Its Implications in Fish Farming in Lake Buluan, Mindanao, Philippines. Polish Journal of Environmental Studies. **33** (1), 391, **2024**.
41. MUHAR S., SCHWARZ M., SCHMUTZ S., JUNGWIRTH M. Identification of rivers with high and good habitat quality: methodological approach and applications in Austria. Hydrobiologia. **422**, 343, **2000**.
42. LI Y., XU Z., MA H., HURSTHOUSE A. Removal of Manganese(II) from Acid Mine Wastewater: A Review of the Challenges and Opportunities with Special Emphasis on Mn-Oxidizing Bacteria and Microalgae. Water. **11**, 2493, **2019**.
43. AYAR M.K., LIANG W., NIAZI Z., IFTIKHAR F. Insights into the Physico-Chemical Parameters of Surface Water and Their Impact on Water Quality and the Pollution. Polish Journal of Environmental Studies. **2025**.
44. ALKAN H., GUL-GUVEN R., GUVEN K., ERDOGAN S., DOGRU M. Biosorption of Cd^{+2}, Cu^{+2}, and Ni^{+2} Ions by a Thermophilic Haloalkalitolerant Bacterial Strain (KG9)

Immobilized on Amberlite XAD-4. Polish Journal of Environmental Studies. **24** (5), 1903, **2015**.
45. HAN C., HAO Y., LIU K., ZHAO H., CHEN W., LIU X. Analysis of Influencing Factors of Rainfall Infiltration Slope Sensitivity Based on Grey Relational Analysis. Polish Journal of Environmental Studies. **34** (1), 671, **2025**.
46. PAŚMIONKA I.B., BULSKI K., HERBUT P., BOLIGŁOWA E., VIEIRA F.M.C., BONASSA G., BORTOLI M., PRÁ M.C.D. Toxic Effect of Ammonium Nitrogen on the Nitrification Process and Acclimatisation of Nitrifying Bacteria to High Concentrations of NH4-N in Wastewater. Energies. **14** (17), 5329, **2021**.
47. WU X., LUO Q., ZHOU Z., ZHU S., MA J., LUO X., HUANG F. Study on the Influence of Expressway Construction on Soil Environment in Karst Area of Guangxi, Southwest China. Polish Journal of Environmental Studies. **2025**.
48. LV Y., ZHU X., ZHANG M., LIU X., WANG J. In-situ Bioremediation of Multiple Heavy Metals Contaminated Farmland Soil by Sulfate-Reducing Bacteria. Polish Journal of Environmental Studies. **31**(2), 1747, **2022**.
49. CHEN Y., XIANG L., LI F., CHEN Y., XIANG L., LI F., CHANG Y., YU H., ZHANG J., XIE Z. The Appropriate Reduction of Nitrogen Fertilization Enhances Soil Quality without Compromising Fruit Yield and Quality in a Bayberry Orchard. Polish Journal of Environmental Studies. **2025**.
50. XIE G.D., ZHANG C.X., ZHEN L., ZHANG L.M. Dynamic changes in the value of China's ecosystem services. Ecosystem Services. **26**, 146, **2017**.
51. GUAN S., QIU S., MEI M., HAO X., ZHANG X., LU X. Assessment of Appropriate Reference Genes for Quantitative Real-Time Polymerase Chain Reaction Normalisation in Magnolia sieboldii K. Koch across Various Experimental Conditions. Polish Journal of Environmental Studies. **31** (3), **2022**.
52. LU Z.D., ZHANG Z.F. Dynamics of Territorial Spatial Pattern and Landscape Impact under Different Economic Gradients: A Case Study of the Beijing-Tianjin-Hebei (BTH) Region, China. Sustainability. **15** (1), 23, **2023**.
53. CHEN S., CHEN G. Spatial Distribution Characteristics and Human Health Risk Assessment of Heavy Metal Pollution in Chao hu Lake. Polish Journal of Environmental Studies. **2025**.
54. LIU Y., MA J., CHEN K., LIU Q., CHAI H., ZHANG H. Heavy Metals Pollution Evaluation, Health Risk Assessment, and Source Identification in the Reservoirs, Northern Anhui Province, China. Polish Journal of Environmental Studies. **2024**.
55. CHEN H.J. The ecosystem service value of maintaining and expanding terrestrial protected areas in China. Science of the Total Environment. **781**, 10, **2021**.
56. ZHANG L.F., FANG C.L., ZHAO R.D., ZHU C., GUAN J.Y. Spatial-temporal evolution and driving force analysis of eco-quality in urban agglomerations in China. Science of the Total Environment. **866**, 14, **2023**.
57. DENG W., LIU M., HAN C., ZHAO L., YUTING Z., YUAN H., MINGLI W., LUYI N. Spatial Distribution Characteristics and Source Analysis of Ions in Lancang River and Yangtze River Source Region During Wet Period. Polish Journal of Environmental Studies. **33** (5), 5597, **2024**.
58. WANG G., LI T., YIN W., ZHOU J., LU D. Effect of Sodium Hypochlorite Disinfection on Polyvinylidene Fluoride Membranes in Microplastic Ultrafiltration. Water. **17**, **2025**.
59. MA H., ZHAO Y. Environmental Social and Governance Performance, Total Factor Productivity and Environmental Uncertainty in Heavily Polluting Companies. Polish Journal of Environmental Studies. **2025**.
60. DAHOU ME A., DEHMANI S., DEHMANI C., ZERROUKI D. Production and Characterization of Chlorella pyrenoidosa Biomass Cultivated in Domestic Wastewater. Polish Journal of Environmental Studies. **34** (5), **2025**.